

Hidden Population III Descendants in Ultra-Faint Dwarf Galaxies

MARTINA ROSSI ,^{1,2,3} STEFANIA SALVADORI ,^{3,4} ÁSA SKÚLADÓTTIR ,³ IRENE VANNI ,^{3,4} AND IOANNA KOUTSOURIDOU ,³

¹Dipartimento di Fisica e Astronomia “Augusto Righi”, Alma Mater Studiorum, Università di Bologna, Via Gobetti 93/2, 40129 Bologna, Italy

²INAF – Osservatorio di Astrofisica e Scienza dello Spazio di Bologna, Via Gobetti 93/3, 40129 Bologna, Italy

³Dipartimento di Fisica e Astrofisica Università degli Studi di Firenze, via G. Sansone 1, Sesto Fiorentino, Italy

⁴INAF/Osservatorio Astrofisico di Arcetri, Largo E. Fermi 5, I-50125 Firenze, Italy

(Received 18 June, 2024)

ABSTRACT

The elusive properties of the first (Pop III) stars can be indirectly unveiled by uncovering their true descendants. To this aim, we exploit our data-calibrated model for the best-studied ultra-faint dwarf (UFD) galaxy, Boötes I, which tracks the chemical evolution (from carbon to zinc) of individual stars from their formation to the present day. We explore the chemical imprint of Pop III supernovae (SNe), with different explosion energies and masses, showing that they leave distinct chemical signatures in their descendants. We find that UFDs are strongly affected by SNe-driven feedback resulting in a very low fraction of metals retained by their gravitational potential well (< 2.5%). Furthermore, the higher the Pop III SN explosion energy, the lower the fraction of metals retained. Thus, the probability to find descendants of energetic Pair Instability SNe is extremely low in these systems. Conversely, UFDs are ideal cosmic laboratories to identify the fingerprints of less massive and energetic Pop III SNe through their [X/Fe] abundance ratios. Digging into the literature data of Boötes I, we uncover three hidden Pop III descendants: one mono-enriched and two multi-enriched. These stars show the chemical signature of Pop III SNe in the mass range $[20 - 60] M_{\odot}$, spanning a wide range in explosion energies $[0.3 - 5] 10^{51}$ erg. In conclusion, Pop III descendants are hidden in ancient UFDs but those mono-enriched by a single Pop III SN are extremely rare. Thus, self-consistent models such as the one presented here are required to uncover these precious fossils and probe the properties of the first Pop III supernovae.

Keywords: Population III stars — Population II stars — Chemical abundances — Dwarf galaxies

1. INTRODUCTION

A few hundred million years after the Big Bang, in the middle of the Dark Ages, the first (Pop III) stars lit up the Universe initiating its radical transformation. Pop III stars produced the first ionizing photons and while evolving as supernovae (SNe) they injected the first heavy elements, i.e., metals, into the surrounding gas. Understanding the properties of these first cosmic sources, such as their Initial Mass Function (IMF) and the explosion energy of Pop III SNe, is thus crucial to study the early phases of reionization and metal enrichment.

The first stars are predicted to form at redshift $z \sim 20 - 30$ in *minihaloes* of primordial composition gas and thus to be metal-free (e.g. Abel et al. 2002; Bromm 2013). Owing to the lack of efficient coolants in their birth environment, which implies more massive proto-stellar gas clouds (e.g. Bromm et al. 2001; Omukai et al. 2005) and higher gas accretion rate onto the proto-star (Omukai & Palla 2001), we

expect Pop III stars to be more massive than present-day stars, reaching masses up to $1000 M_{\odot}$ (e.g. Tan & McKee 2004; Susa et al. 2014; Hirano et al. 2014). Nevertheless, some 3D hydrodynamical simulations show that zero-metallicity gas clouds can fragment in sub-solar clumps (e.g. Greif et al. 2011; Prole et al. 2022; Riaz et al. 2023), possibly leading to the formation of clusters of low-mass long-lived Pop III stars, which can survive until the present day - but see also Sharda et al. (2021) for different findings. However, these 3D simulations can only follow the first star formation for a very short time ($\approx 10^3$ yr). Thus, on longer time-scales, the frequent mergers experienced by these clumps (e.g. Hirano & Bromm 2017), combined with the high accretion rate of the pristine gas onto the proto-stars, likely led to the formation of massive and very massive Pop III stars (e.g., see Klessen & Glover 2023, for a recent review).

From an observational prospective, the idea that Pop III stars are more massive than present-day stars is supported

by the persistent lack of Pop III survivors. Despite intensive searches, no metal-free stars have been observed in the Local Universe, suggesting that if low-mass long-lived Pop III stars ($m_\star < 0.8 M_\odot$) exist they must be extremely rare (e.g. [Salvadori et al. 2007](#); [Hartwig et al. 2015](#); [Magg et al. 2019](#); [Rossi et al. 2021](#)). In conclusion, the Pop III IMF was almost certainly different than the present-day one and it was possibly biased towards more massive stars, with a characteristic mass, $m_{ch} > 1 M_\odot$ (e.g. [de Bennassuti et al. 2017](#); [Sarmento et al. 2019](#); [Rossi et al. 2021](#); [Pagnini et al. 2023](#)).

If Pop III stars are predominantly massive, then most of them are expected to evolve in a few Myr exploding as SNe and polluting the surrounding interstellar medium (ISM) with their newly produced chemical elements. In the mass range $m_\star = [10 - 100] M_\odot$, each Pop III SNe can evolve with very different explosion energy, from $E_{SN} \approx 10^{50}$ erg to $E_{SN} \approx 10^{52}$ erg (e.g. [Heger & Woosley 2010](#); [Kobayashi et al. 2006](#)). Conversely, very massive Pop III stars, $m_\star = [140 - 260] M_\odot$, explode as powerful Pair Instability Supernovae (PISN), with an energy that increases with their progenitor mass ([Heger & Woosley 2002](#); [Takahashi et al. 2018](#)). The amount and composition of new elements produced and injected in the ISM by these first Pop III SNe depend upon both the progenitor mass and the SNe explosion energy (see e.g. [Vanni et al. 2023](#)).

The chemical signatures of these pristine SNe can be retained in the photospheres of ancient, low-mass Pop II stars that formed from “the ashes” of these massive first stars.

In the Local Group, the pursuit of identifying the descendants of Pop III stars has yielded fruitful results, enabled by the capacity to observe and resolve individual stars. Among ancient very metal-poor stars ($[Fe/H] < -2$), the most promising candidates are the so called Carbon-Enhanced Metal Poor - no (CEMP-no) stars, which are characterized by $[C/Fe] > +0.7$ (e.g. [Beers & Christlieb 2005](#); [Bonifacio et al. 2015](#)) and no excess in neutron-capture elements, $[Ba/Fe] < 0$. Various studies have shown a connection between CEMP-no stars and the chemical elements produced by Pop III stars ([Iwamoto et al. 2005](#); [Ishigaki et al. 2014](#)), in particular those that explode as *faint supernovae* ($E_{SN} < 10^{51}$ erg). On the other hand, the Pop III descendants imprinted by *energetic* pristine SNe ($E_{SN} > 10^{51}$ erg) have been found both among CEMP-no stars and Carbon-normal, $[C/Fe] < +0.7$, stars: [Ezzeddine et al. \(2019\)](#) identified the fingerprints of asymmetric *hypernova* with $E_{SN} = 5 \times 10^{51}$ erg in the CEMP-no star HE 1327-2326 at $[Fe/H] \approx -5$ and more recently, [Skúladóttir et al. \(2021\)](#) and [Placco et al. \(2021\)](#) discovered two C-normal metal-poor stars ($[Fe/H] < -4$) in the Sculptor dwarf galaxy and in the Galactic halo, respectively, whose

abundance patterns are compatible with an enrichment by a Pop III *hypernova*, with $E_{SN} = 10 \times 10^{51}$ erg.

Despite these discoveries at extremely low-metallicities, models predict that the probability to find direct descendants of high-energy Pop III SNe increases towards higher $[Fe/H]$ ([Vanni et al. 2023](#)). However, their detection becomes more challenging at higher $[Fe/H]$ due to the increasing numbers of subsequent generations of Pop II descendants there ([Salvadori et al. 2015](#); [de Bennassuti et al. 2017](#); [Hartwig et al. 2018](#); [Koutsouridou et al. 2023](#)). For example, the descendants of PISN are expected to appear in a very broad metallicity range $-4 < [Fe/H] < -1$ with a peak at $[Fe/H] \approx -1.8$ ([Karlsson et al. 2013](#); [de Bennassuti et al. 2017](#); [Salvadori et al. 2019](#); [Koutsouridou et al. 2024](#)). Indeed, several candidate PISN descendants have been found at $[Fe/H] \approx -2$ ([Aguado et al. 2023](#)) including the one identified by ([Xing et al. 2023](#)), whose abundance pattern is unfortunately not anymore consistent with a pure PISN enrichment ([Skúladóttir et al. 2024](#); [Thibodeaux et al. 2024](#)).

In conclusion, the precious Pop III descendants are expected to appear in a wide range of metallicity from $[Fe/H] \approx -1$ down to $[Fe/H] \approx -7$ and among both CEMP and C-normal stars.

Among all environments hosting ancient stars, Ultra-Faint Dwarf galaxies (UFDs) stand out as ideal systems for studying the nature of the first stars and catching the chemical fingerprints of the first SNe ([Salvadori & Ferrara 2009](#); [Salvadori et al. 2015](#); [Magg et al. 2017](#); [Hartwig & Yoshida 2019](#); [Rossi et al. 2021, 2023](#)). From a theoretical perspective, these low-mass dwarf galaxies are compelling candidates for being the building blocks of present-day galaxies, such as our Milky Way, and the first star forming systems hosting Pop III stars ([Salvadori et al. 2015](#)). Observationally, they are the oldest, most dark matter-dominated, most metal-poor, least luminous ($L_{bol} < 10^5 L_\odot$), and least chemically evolved stellar systems known ([Simon 2019](#)). The majority of UFDs formed more than 75% of their stars within the first billion years of their evolution, resulting in truly ancient stellar populations, with ages exceeding 12 Gyr ([Brown et al. 2014](#); [Gallart et al. 2021](#)). Furthermore, UFDs harbor the highest fraction of very metal-poor stars ($[Fe/H] < -2$), with a significant portion of CEMP-no stars ([Kirby et al. 2013](#); [Yong et al. 2013](#); [Spite et al. 2018](#); [Yoon et al. 2019](#)). Finally, the observed stars in UFDs display a broad metallicity range of $-4 < [Fe/H] < -1$ ([Fu et al. 2023](#)). These properties make UFDs compelling laboratories to search for the chemical imprints of Pop III SNe with different energies, ranging from *faint* ($E_{SN} \approx 10^{50}$ erg) SNe up to PISN ($E_{SN} > 10^{52}$ erg).

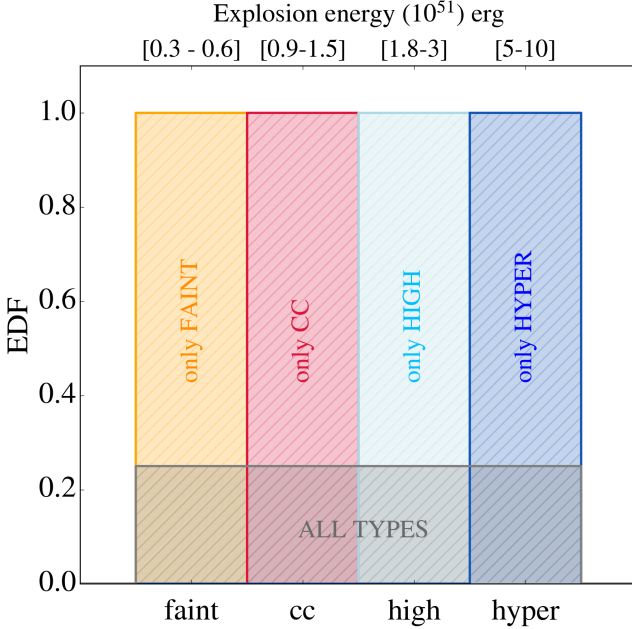


Figure 1. Assumed EDFs: four cases in which the EDF is a top-hat function centered on each type of SNe (100% probability), and the last case in which all SNe explosion energies are equiprobable (25% probability of each type)

In this work, we investigate the chemical signatures of Pop III SNe with different energies and masses, in UFD galaxies especially focusing on one of the most luminous and best studied, Boötes I.

2. MODEL DESCRIPTION

The data-calibrated model used in this work was first introduced in Rossi et al. (2021) and expanded in Rossi et al. (2023). The aim of the model is to describe the chemical evolution of an UFD, particularly focusing on the best studied system: Boötes I. This semi-analytical model follows the star formation and chemical enrichment history of Boötes I from its formation epoch to the present day, by tracking elements from carbon to zinc produced by both Pop III and Pop II/I stars. The model can be summarized as follows (for details see Rossi et al. 2021, 2023):

Initial conditions: We assume Boötes I to evolve in isolation, i.e. without experiencing major merger events. This is consistent with cosmological models (Salvadori & Ferrara 2009; Salvadori et al. 2015), which are used to set the initial conditions: the epoch of virialization, $z_{\text{vir}} \approx 8.5$, and the dark-matter halo mass, $M_h \approx 10^{7.3} M_\odot$.

Star formation: At the virialization epoch we compute the total amount of gas¹ as $M_g = \Omega_b / \Omega_m M_h$, and we assume it to be pristine. The star-formation becomes possible when the gas begins to fall into the central part of the halo and cool down (see Rossi et al. 2021, for the infall rate). We evaluate the total mass of stars formed in a timescale of 1 Myr, assuming a star-formation rate regulated by the free-fall time (t_{ff}) and the mass of cold gas accumulated via infall (M_{cold}): $\Psi = \epsilon_\star M_{\text{cold}} / t_{\text{ff}}$, where ϵ_\star is a free parameter of the model, equal for both Pop III and Pop II/I stars.

Following the critical metallicity scenario (Bromm et al. 2001; Schneider et al. 2003; Omukai et al. 2005), Pop III stars only form if the metallicity of the ISM gas², Z_{gas} , is below the critical metallicity, $Z_{\text{cr}} = 10^{-4.5 \pm 1} Z_\odot$, i.e. $Z_{\text{gas}} \leq Z_{\text{cr}}$, while *normal* Pop II/I stars form when $Z_{\text{gas}} > Z_{\text{cr}}$.

Initial Mass Function (IMF): We assume the newly-formed stellar mass to be distributed according to an Larson IMF (Larson 1998):

$$\phi(m_\star) = \frac{dN}{dm_\star} \propto m_\star^{-2.35} \exp(-m_{ch}/m_\star) \quad (1)$$

where m_\star is the stellar mass and m_{ch} the characteristic mass of the IMF. For Pop III stars $m_{ch} = 10 M_\odot$ and $m_\star = [0.8 - 1000] M_\odot$ (consistent with the results of Hirano et al. 2014; Hirano & Bromm 2017; Rossi et al. 2021; Pagnini et al. 2023); while for Pop II stars $m_{ch} = 0.35 M_\odot$ and $m_\star = [0.1 - 100] M_\odot$.

The model includes the incomplete sampling of the stellar IMF for both Pop III and Pop II stellar populations. Every time that the conditions for star formation are reached, a discrete number of stars is formed, with mass selected randomly from the assumed IMF. This is a key feature of the model, essential for accurately simulating the evolution of poorly star-forming UFDs in which the assumed IMF is never fully sampled throughout its entire evolution (see Rossi et al. 2021).

Chemical feedback: The chemical enrichment of the gas is followed by taking into account the mass-dependent timescales for the evolution of individual stars. In particular, the semi-analytical model tracks and follows the chemical elements (from carbon to zinc) released by SNe and AGB stars from both the Pop III and Pop II/I stellar populations.

¹We adopt Λ cold dark matter (Λ CDM) with $h = 0.669$, $\Omega_m = 0.3103$, $\Omega_\Lambda = 0.6897$, $\Omega_b h^2 = 0.02234$, $\sigma_8 = 0.8083$, $n = 0.9671$, according to the latest Plank results (Planck Collaboration et al. 2018)

² $Z_{\text{gas}} = M_Z^{\text{ISM}} / M_{\text{gas}}$ where M_Z^{ISM} and M_{gas} are the mass of metals and gas in the ISM, respectively.

- SNe can enrich the ISM with all chemical elements from carbon to zinc. For Pop III SNe in the mass range $m_{\text{Pop III}} = [10 - 100] M_{\odot}$ we use the stellar yields from Heger & Woosley (2010), while for massive PISN we adopt the ones of Heger & Woosley (2002) in the mass range $m_{\text{PISN}} = [140 - 260] M_{\odot}$. For Pop II/I SNe in the mass range $[8 - 40] M_{\odot}$ we use the updated metal yields of Limongi & Chieffi (2018), model R, without rotation and with a fixed explosion energy $E_{\text{SN}} = 10^{51} \text{ erg}$.
- AGB stars in the mass range $[2 - 8] M_{\odot}$ enrich the ISM through stellar winds, only in carbon, nitrogen, and oxygen. We adopt the stellar yields of Meynet & Maeder (2002) (rotating model) for Pop III stars, and van den Hoek & Groenewegen (1997) for Pop II/I stars.

Mechanical feedback: Stars that end their lives as SNe not only pollute the ISM with heavy elements but can also enrich the intergalactic medium (IGM) through mechanical feedback. Indeed, SNe explosions can generate a blast wave that, when sufficiently energetic, can overcome the gravitational potential well of the host halo, resulting in the expulsion of gas and metals into the IGM. The ejected mass, M_{ej} is regulated by: $M_{\text{ej}} = (2\epsilon_w N_{\text{SN}} E_{\text{SN}})/v_{\text{esc}}^2$ (see Salvadori et al. 2008). Here, $\epsilon_w N_{\text{SN}} E_{\text{SN}}$ is the total kinetic energy injected into the halo, N_{SN} the number of SNe, E_{SN} the explosion energy, and ϵ_w is a free parameter, which controls efficiency of the SNe-driven winds. The escape velocity of the gas depends on the halo mass, M_h , and viral radius of the halo (see Barkana & Loeb 2001)). The metals injected into the ISM by SNe undergo complete mixing with the halo gas, so the metallicity of the ejected gas is the same as that of the ISM.

Energy Distribution Function (EDF) of Pop III SNe: For $(10 - 100) M_{\odot}$ Pop III stars ending their lives as SNe, we follow Heger & Woosley (2010) and explore different possible explosion energies :

- *faint* SNe: $E_{\text{SN}} = [0.3 - 0.6] \times 10^{51} \text{ erg}$;
- *core-collapse (cc)* SNe: $E_{\text{SN}} = [1.2 - 1.5] \times 10^{51} \text{ erg}$;
- *high-energy* SNe: $E_{\text{SN}} = [1.8 - 3.0] \times 10^{51} \text{ erg}$;
- *hypernovae*: $E_{\text{SN}} = [5.0 - 10.0] \times 10^{51} \text{ erg}$;

We explore five different possibilities for the unknown EDF of Pop III SNe, shown in Fig. 1. In the first four cases we assume extreme scenarios in which Pop III SNe are all of a single type: *only faint*, *only cc*, *only high*, or *only hyper*. This corresponds to a top-hat EDF in which the probability to form the chosen type of SNe is 100%. In the last case we assume an EDF spread among all different explosion energies (“all types” model), where each SNe type has an equal probability

of 25%. Thus, every time a Pop III SN progenitor forms we randomly assign to it an explosion energy.

Conversely, in the mass range $[140 - 260] M_{\odot}$, we assume that Pop III stars evolve as PISNe with an explosion energy $E_{\text{SN}} = [10, 100] \times 10^{51} \text{ erg}$, proportional to the stellar mass (Heger & Woosley 2002), and therefore *independent* from the assumed EDF for SNe with less massive progenitor stars. Note that the probability to form PISNe is regulated by both the assumed Pop III IMF and the star-formation rate, which affect the random sampling of the Pop III IMF (see Rossi et al. 2021). Assuming a fully sampled Pop III IMF we obtain that this probability is $\sim 0.2\%$.

Data Calibration: The model is data-calibrated: the free parameters ($\epsilon_{\star}, \epsilon_w$) have been fixed to reproduce the observed properties of the Boötes I UFD, i.e. the total luminosity, L_{bol} , the average stellar iron-abundance, $\langle [\text{Fe}/\text{H}] \rangle$, and the star formation history (for details see Rossi et al. 2021). Due to the stochastic nature of the IMF sampling, the chemical enrichment history of Boötes I can vary between different runs of the code. For this reason, all the results presented here have been obtained by averaging over 1000 possible Boötes I evolutionary histories and by quantifying the scatter among them.

3. THE ENERGY DISTRIBUTION OF POP III SNE: IMPACT

As a first step we investigate how the predicted properties of Boötes I change by assuming different EDFs of Pop III SNe, as defined in the previous Section (Fig. 1). While the predicted $\langle [\text{Fe}/\text{H}] \rangle$, L_{bol} and star formation history of Boötes I, are minimally influenced by the assumed EDF of Pop III SNe, as we shall now see, the Metallicity Distribution Function (MDF) is notably impacted. For this reason, we use a χ^2 procedure to quantify which is the best model, among those assuming different EDFs, that reproduces the observed MDF of Boötes I, along with its global properties i.e. $\langle [\text{Fe}/\text{H}] \rangle$, and L_{bol} .

Firstly, we consider that SNe in the mass range $[10 - 100] M_{\odot}$ are all of a unique type. Then we relax this assumption and assume a flat EDF in which the four SNe types have the same probability (25%). The impact of the different Pop III EDFs on the MDF of Boötes I is shown in Fig. 2. The χ^2 values for the different models are reported in Table 1.

The models “only faint”, and “only hyper” have a high $\chi^2 > 1$, and are thus disfavored. Since faint SNe produce large amounts of C and small of Fe, they result in a long low-Fe tail in the MDF which is not observed in Boötes I (see Fig. 2), and therefore the “only faint” model is less favoured. On the other hand, assuming that all Pop III SNe explode as hypernovae shifts the peak of the MDF towards lower $[\text{Fe}/\text{H}]$ values. Indeed, due to the low potential well of Boötes I, when

	$\log(L_\star/L_\odot)$	$\langle [\text{Fe}/\text{H}] \rangle$	χ^2
Boötes I	4.50 ± 0.10	-2.58 ± 0.43	-
FAINT	4.60 ± 0.01	-3.00 ± 0.01	1.5
CC	4.59 ± 0.02	-2.60 ± 0.01	0.9
HIGH	4.60 ± 0.01	-2.68 ± 0.03	0.4
HYPER	4.40 ± 0.01	-3.20 ± 0.01	4.8
all TYPES	4.54 ± 0.04	-2.70 ± 0.01	0.5

Table 1. Observed properties of Boötes I (top row; Kirby et al. 2013; Norris et al. 2010; Lai et al. 2011; Gilmore et al. 2013), and the simulated properties with their corresponding χ^2 values, by adopting the different EDFs for Pop III SNe from Fig. 1.

all Pop III explode as energetic hypernovae the majority of the gas and metals are evacuated out of the galaxy. As a result, retaining metals in the halo becomes challenging. In addition, due to the lack of available gas for star formation, the star formation rate of subsequent Pop II is very low ($\Psi \approx 10^{-3} M_\odot \text{yr}^{-1}$), leading to less efficient metal enrichment.

The other three models give $\chi^2 < 1$. The lowest χ^2 value is for the “only high” model, however, the difference in χ^2 is not enough to distinguish between models: $\chi^2 = 0.9$ (only cc), $\chi^2 = 0.4$ (only high), and $\chi^2 = 0.5$ (all types). Therefore, we need to include other observables of the Boötes I UFD to select our “fiducial” model.

In Fig. 3 we analyze how the different EDFs for Pop III SNe affect the predicted abundance ratios³ of present-day stars in Boötes I. In particular we focus on [C/Fe] and [Zn/Fe], which are very sensitive to different explosion energies. For each model, the contours delineate the stellar populations that have been *predominantly imprinted* by a unique type of Pop III SNe, i.e., that contributed $> 75\%$ of their present-day mass in metals.

The location of these Pop III descendants in the [X/Fe]–[Fe/H] space depends on both the energy and on the progenitor mass of the Pop III SNe that enriched their birth clouds (see also Vanni et al. 2023). However, we can notice that the descendants of low-energy Pop III SNe (faint, cc) cover a wide range in both [Fe/H] and [C/Fe], $-7.5 \lesssim [\text{Fe}/\text{H}] \lesssim 0$, and, $-1 \lesssim [\text{C}/\text{Fe}] \lesssim 6$, and they are characterized by $[\text{Zn}/\text{Fe}] \lesssim 0$. On the other hand, Pop III descendants which are predominantly enriched by energetic SNe (high and hypernovae) exhibit a narrower range in $-1 \lesssim [\text{C}/\text{Fe}] \lesssim 3$ and $-4 < [\text{Fe}/\text{H}] < 0$. Note that only stars imprinted by high energy SNe and hypernovae can reach super-solar [Zn/Fe] values, up to $\approx +1$ dex. Finally, in Fig. 3 we also show the regions covered by stars enriched by *normal*

³ $[\text{X}/\text{Fe}] = \log(N_{\text{X}}/N_{\text{Fe}}) - \log(N_{\text{X},\odot}/N_{\text{Fe},\odot})$; where N_{X} and N_{Fe} are the abundances of elements X and Fe, and $N_{\text{X},\odot}$ and $N_{\text{Fe},\odot}$ are the solar values (Asplund et al. 2009)

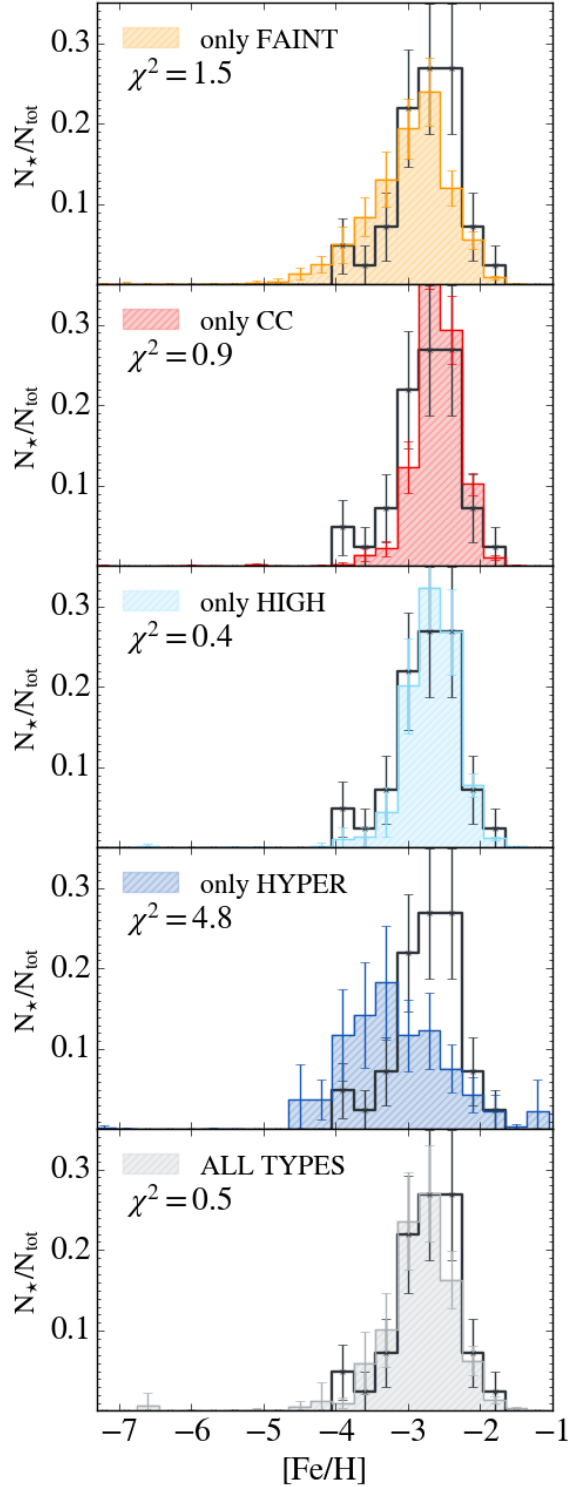


Figure 2. Comparison between the observed (black histograms) and the simulated MDFs of Boötes I. The top four simulated MDFs are obtained assuming that Pop III SNe are all of a single type: faint (orange), core-collapse (cc, red), high (light blue), hyper (dark blue). Bottom panel shows the simulated MDF obtained assuming a flat EDF spread among all energies (gray). In each panel the goodness of the fit, χ^2 , is shown (see also Table 1).

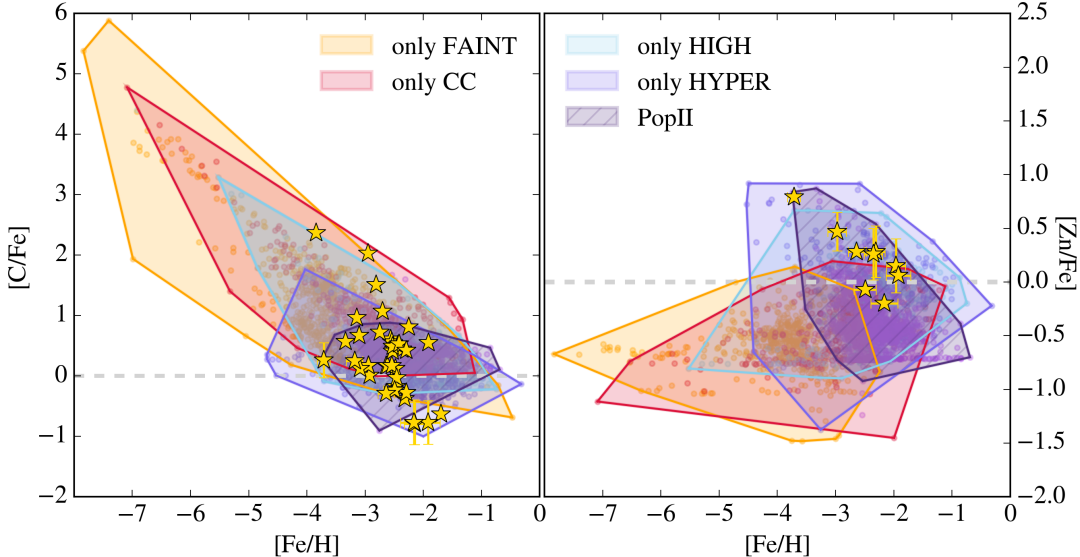


Figure 3. The $[C/Fe]$ (left panel) and $[Zn/Fe]$ (right panel) abundance ratio of Boötes I stars (yellow stars) as a function of their $[Fe/H]$ (SAGA Database Suda et al. (2008)). Colored contours identify the the stellar populations enriched to a level higher than 75% by Pop III SNe with different energies, *faint* (orange), *cc* (red), *high* (lightblue), *hyper* (dark blue). For comparison we also show the expected chemical abundance ratios of stellar population mainly enriched by *normal* Pop II SNe (dark purple shaded area). Note that the scales on the y-axis are different in the two panels.

Pop II SNe, which typically have $[C/Fe] \lesssim 1$ and they can reach high values of $[Zn/Fe] \gtrsim 0$, comparable with those obtained with hypernovae enrichment.

Which EDF for Pop III SNe can reproduce the observed $[C/Fe]$ and $[Zn/Fe]$ ratios of Boötes I stars? From comparing our model results with observational data for Boötes I (Fig. 3) it is evident that *none of the individual models* which assume a single Pop III SNe type (only faint/cc/high/hyper) is able to reproduce, at the same time, the observed distributions of $[C/Fe]$ and $[Zn/Fe]$. In fact, assuming that all pristine SNe evolve as low-energy SNe allows to reproduce the high values of $[C/Fe]$ observed in Boötes I stars but not the high $[Zn/Fe]$ values. On the other hand, energetic SNe can reproduce the measured values of $[Zn/Fe]$, but fail to reproduce the observed $[C/Fe]$ stellar ratios. Finally, even taking into account the contribution of Pop II SNe, it is not possible to reproduce the data, as well as assuming a single type of Pop III SNe.

In conclusion, to reproduce the variety of $[C/Fe]$ and $[Zn/Fe]$ measured in Boötes I stars with different $[Fe/H]$ we need the contribution of Pop III SNe with different energies. Thus, we choose as our “*fiducial model*” the “all types” model (see Fig. 1) in which the theoretical EDF is spread among different equiprobable energies.

4. EARLY CHEMICAL EVOLUTION: PREDICTIONS

In Fig. 4, we show all the predicted $[X/Fe]$ versus $[Fe/H]$ density maps for the present-day stellar populations in Boötes I predicted by our *fiducial model* (“all types” in

Fig. 1). The first thing to note is that all the simulated $[X/Fe]$ density maps effectively reproduce the observed data. Indeed, the peaks of the simulated density distributions for each chemical element perfectly match the corresponding observed distributions. It is worth mentioning that the simulated density maps include many more stars than those observed, and cover a broader range in the $[X/Fe]$ - $[Fe/H]$ space. Our model predicts regions of low density (< 20% of the density peak), representing rare stellar populations, not yet observed in UFDs, that are particularly intriguing for investigating the signatures of the first stars.

In the top marginal plots of Fig. 4 we compare the normalized MDFs of Boötes I observed and simulated, including the predicted MDFs for stars predominantly enriched by Pop III ($> 75\%$ of their metals, top right) and by Pop II stars (top left). In the range where data are available, $[Fe/H] > -4$, the simulated MDF is dominated by stars predominantly enriched by normal Pop II SNe. Indeed, Pop II enriched stars represent $> 90\%$ of the total number of stars in these $[Fe/H]$ range, while stars mainly imprinted by Pop III SNe are extremely rare at $[Fe/H] > -4$, only counting for $\approx 1\%$ of the total population. On the other hand, in the low-metallicity tail of the MDF ($[Fe/H] < -4$), the number of stars that inherited $> 75\%$ of their metals from Pop III SNe is of the same order of magnitude as those predominantly enriched by Pop II. As we shall now see, for $[Fe/H] < -4$, Pop III descendants can be distinguished from Pop II enriched stars as *outliers*, i.e., thanks to their key $[X/Fe]$ abundance ratios.

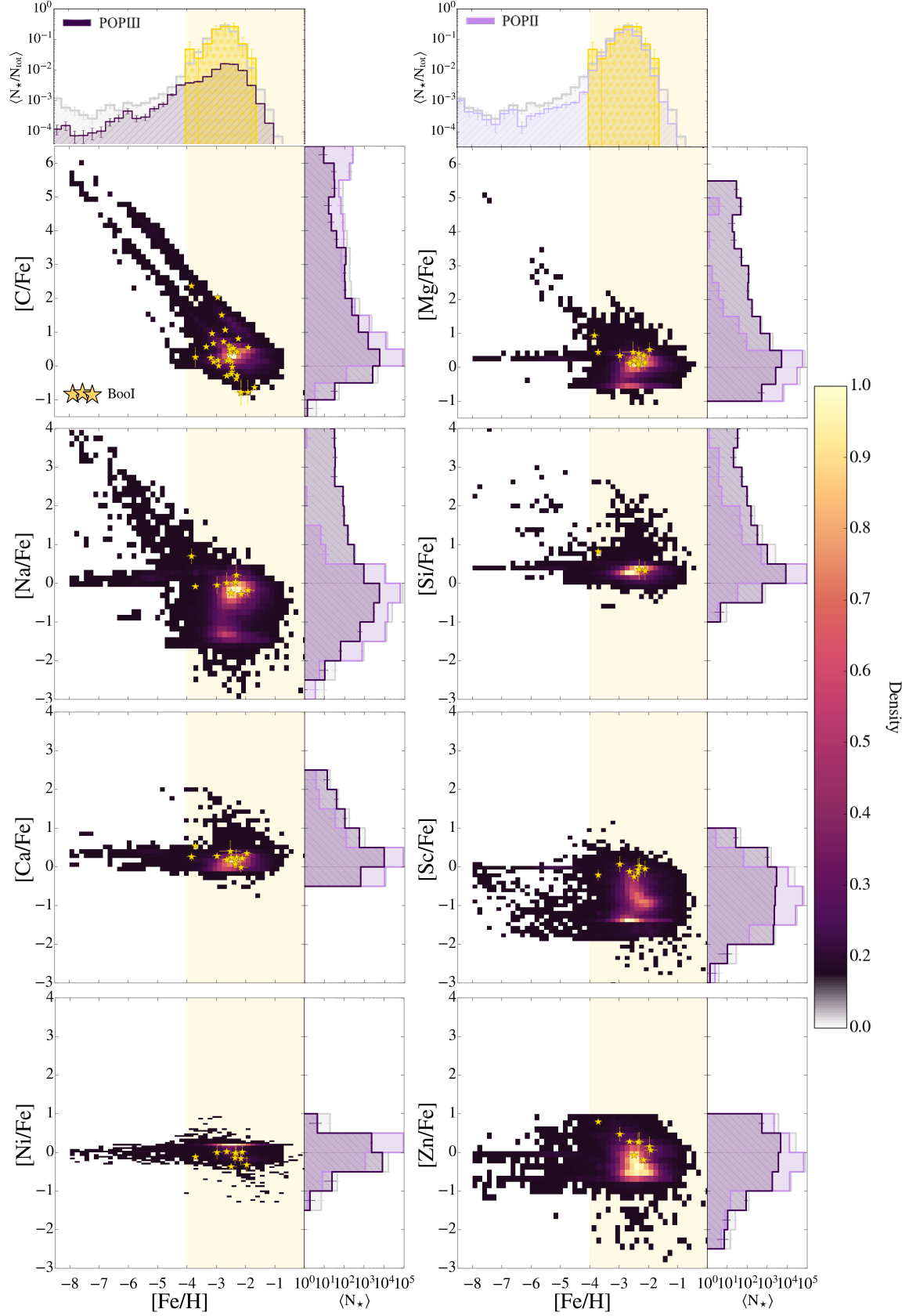


Figure 4. Density maps, $[X/Fe] - [Fe/H]$, of the simulated stellar populations at present day, $z = 0$. Yellow star symbols are observed chemical abundances of Boötes I stars (SAGA Database Suda et al. (2008)). Top marginal histograms show the MDFs of: observed Boötes I stars (yellow), all stars (light grey), stars enriched at level higher than 75% by Pop III stars (dark purple, top left) and stars enriched at level higher than 75% by Pop II stars (light purple, top right). Right marginal plots show the $[X/Fe]$ abundance ratio distributions for: all simulated stars (light grey), and predominantly ($> 75\%$) Pop III/Pop II enriched stars (dark/light purple). The shaded yellow area highlights $[Fe/H] > -4$.

4.1. Key abundance ratios to unveil Pop III descendants

Now we investigate if there are regions in the $[X/Fe]$ – $[Fe/H]$ space where it is possible to *uniquely* identify the fingerprints of Pop III SNe. To this aim we derive the X-Distribution Function (XDF), i.e. the number of stars in bins of $[X/Fe]$ averaged over different runs, $\langle N_\star \rangle$. In the right marginal plots of Fig. 4, we show the comparison between the total XDF (grey), and the XDFs of stars predominantly ($>75\%$ of their metals) enriched by Pop III (dark purple) or normal Pop II/I stars (light purple).

For all chemical abundance ratios, the peak of the XDF corresponds to the density peak in star formation and thus it is dominated by stellar populations mainly enriched by normal Pop II/I stars as already explained (see also Rossi et al. 2021). In the low density regions, however, the fingerprints of the first SNe arise, i.e. the XDFs are typically dominated by Pop III enriched stars. In conclusion, in the low metallicity regime, $[Fe/H] < -4$, stars characterized by $[C/Fe] \gtrsim +1$ or $[C/Fe] \lesssim 0$, $[Mg/Fe] \gtrsim +0.5$, $[Na/Fe] \gtrsim +0.5$, $[Si/Fe] \gtrsim +1$, $[Ca/Fe] \gtrsim +0.5$, $[Ni/Fe] \gtrsim +0.5$, or $[Zn/Fe] \lesssim -1$ have a high probability ($> 80\%$) to be Pop III descendants.

4.2. The imprints of different Pop III SNe types

According to our model predictions, a large fraction of stars with $[C/Fe] \gtrsim +1$ or $[C/Fe] \lesssim 0$ are likely to be Pop III descendants (Fig. 4). Now we go deeper into understanding the origin of these Pop III descendants, exploring the *type* of SNe that enriched their birth cloud. In Fig. 5 we present the $[C/Fe]$ - $[Fe/H]$ diagram for Boötes I stellar populations predominantly enriched by different Pop III SNe types. As we can see, Pop III descendants can cover a very broad range of both $-7 < [Fe/H] < -1$ and $-1 \lesssim [C/Fe] \lesssim 4$. However, the probability to find them strongly depends on their location in the $[C/Fe]$ - $[Fe/H]$ space, being maximum for $[Fe/H] \lesssim -3.5$ and $[C/Fe] \gtrsim +1$; or when $[Fe/H] \gtrsim -3.5$ and $[C/Fe] \lesssim 0$. This is also illustrated in Fig. 10 (Appendix A), where we show the absolute carbon abundance, $A(C)$, with respect to $[Fe/H]$.

At $[Fe/H] \lesssim -3.5$, around 90% of the stars in Boötes I are predicted to be CEMP stars, in which the carbon enhancement can be driven by both AGB Pop II stars and Pop III SNe. However, Pop III enriched CEMP stars can be identified through their $A(C)$ (see Rossi et al. (2023) and Appendix A). By inspecting the top marginal plots of Fig. 5, where the average number of stars, $\langle N_\star \rangle$, predominantly imprinted by Pop III SNe with different energies is shown, it is evident that the enrichment of CEMP stars can arise from different Pop III sources: faint, cc and high energy SNe. Thus, we can conclude that the progenitors of Pop III enriched CEMP stars in Boötes I can be both low-energy (faint, cc) and high-energy Pop III SNe. Conversely, direct descendants of hypernovae

are uncommon within this range, $[Fe/H] \lesssim -3.5$, and they mainly have $[C/Fe] < 0.7$.

As the $[Fe/H]$ increases, the population of CEMP stars enriched by low-energy Pop III SNe, decreases; while the population of C-normal stars, enriched by energetic (high-energy and hyper) Pop III SNe, increases (see right marginal plot of Fig. 5). Note that, towards high $[Fe/H]$ values, the probability to find descendants of Pop III stars declines due to the chemical pollution of subsequent Pop II stellar populations. Therefore, we expect that the majority of stars with $[Fe/H] \gtrsim -3.5$ have originated from gas that has been enriched by multiple generations of Pop II stars (see Appendix A). Nevertheless, among C-normal stars with $[C/Fe] \lesssim +0.7$ we expect to find the imprints of Pop III SNe of different energies, while the imprint of hypernovae is dominant at $[C/Fe] \lesssim -0.5$, accounting for 6% of the total stars in this range.

4.3. Does Boötes I host stars mono-enriched by Pop III SNe?

Here, we define “mono-enriched” stars as those that have originated from gas enriched by *exactly one* Pop III supernova. Fig. 5 shows that in Boötes I we can potentially find mono-enriched stars which cover wide ranges in $[Fe/H]$ and $[C/Fe]$, and are enriched by different types of Pop III SNe. In line to what we discussed already, for $[C/Fe] > +0.7$ and $[Fe/H] \lesssim -3.5$ we find predominantly mono-enriched stars imprinted by faint, cc, high energy. Mono-enriched CEMP stars are rare $\sim 5\%$ with respect to the total of CEMP stars in Boötes I, and $\sim 5\%$ with respect to CEMP stars predominantly enriched by Pop III. On the other hand, mono-enriched stars by hypernovae are typically found at $[C/Fe] < +0.7$ and $[Fe/H] \gtrsim -3.5$. Their fraction is maximum for $[C/Fe] < -0.5$ representing 10% with respect the total number of stars in this range.

5. PROGENITORS OF INDIVIDUAL BOÖTES I STARS

We can now use the predictions of our chemical evolution model to uncover hidden Pop III descendants in Boötes I. To this end, we analyze the measure abundance patterns of Boötes I stars available in the literature, for which at least five chemical abundance ratios have been measured. To identify the progenitors of Boötes I stars, we compared the abundance patterns of simulated stars that survive until today with those of observed stars. Firstly we pre-selected models that have $[Mg/Fe]$ and $[Fe/H]$ abundance ratios that are consistent with the observed values, i.e., within the error bars. Then, among all models reproducing $[Mg/Fe]$ and $[Fe/H]$, we found those that best fit all the measured chemical elements by minimizing the χ^2 between the simulated and observed $[X/Fe]$ ratios. Finally, after selecting the best fits, we retrieve from the simulation the properties of the SNe responsible for enriching

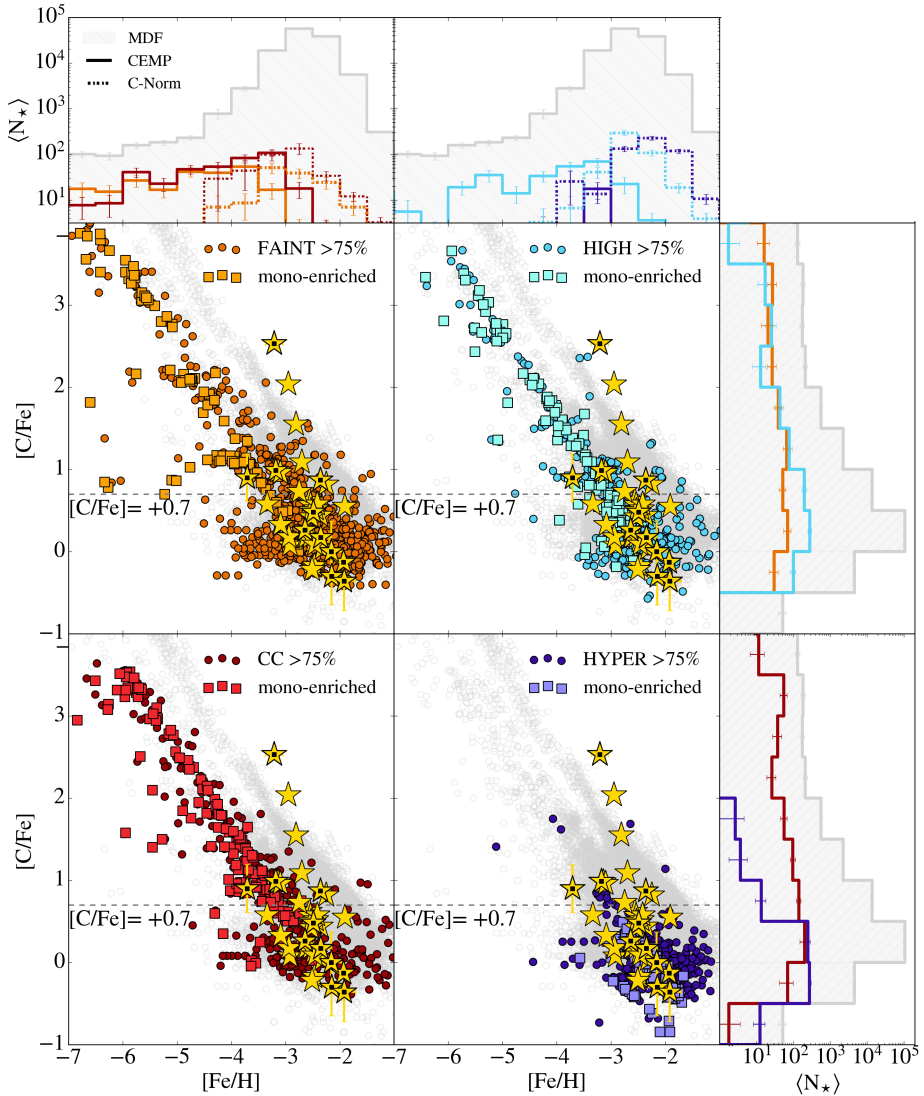


Figure 5. The $[C/Fe]$ vs $[Fe/H]$ diagram of stellar Boötes I stellar populations mainly enriched by Pop III SNe with different energy: low-energy (first column), high-energy (second column). Top marginal plots show the average number of stars, $\langle N_\star \rangle$, as a function of their $[Fe/H]$ of CEMP (solid) and C-normal (dashed) stars enriched at level higher than 75% by different Pop III SNe types, as well as the distribution of overall stars in Boötes I while right marginal plots show $\langle N_\star \rangle$ as a function of $[C/Fe]$. Yellow stars represent the Boötes I data, while double marked points identify stars for which abundance pattern is available in the literature.

the birth cloud from which these stars originated. Note that the $[C/Fe]$ ratio of the observed stars in Boötes I have been corrected for the effect of evolutionary status by exploiting the online tool⁴ presented in Placco et al. (2014), while the abundance ratios are not corrected for 3D and Non-Local

Thermodynamic Equilibrium (NLTE) effects.

We categorized Boötes I stars into the following groups, according to their progenitors: i) *Hidden Pop III descendants*, long-lived stars enriched by Pop III SNe. ii) *Ambiguous stars*, whose abundance patterns are consistent with a predominant enrichment from both Pop III and/or Pop II stars, making it challenging to distinguish between these two scenarios; and

⁴ <http://vplacco.pythonanywhere.com/>

iii) *Pop II descendants*, which are primarily enriched by the normal Pop II stellar population. Below, we will concentrate on the truly/ambiguous Pop III descendants, i.e., groups i) and ii), while in Appendix B we discuss group iii).

5.1. Hidden Pop III descendants

Three stars in Boötes I have abundance patterns consistent with a 100% enrichment from Pop III SNe. When we refer to a 100% enrichment by Pop III SNe, we are indicating that the star formed in an environment enriched solely by Pop III SNe. However, this does not imply that the star has been enriched by a single supernova, i.e. that the star is a mono-enriched Pop III descendant. For this reason, in the following, we will differentiate between multi- and mono-enriched Pop III descendants. The comparison between the measured abundance patterns and the best-fits ones are shown in Fig.6. Additionally, we show the abundance pattern of a star enriched by multiple Pop II stellar populations (100% Pop II enriched star) with the chi-square closest to the minimum.

5.1.1. Mono-enriched Pop III descendants

In Boötes I we uncover one mono-enriched Pop III descendant, i.e. a star imprinted by a single Pop III SNe:

Boo-130: The best fit shows that Boo-130 is mono-enriched by a hypernova with $m_\star = 50 M_\odot$ and $E_{SN} = 10 \times 10^{51}$ erg (Fig.6). Note that in this case, [Zn/Fe] is the key abundance ratio to discriminate between an enrichment driven by Pop III and Pop II stellar populations.

5.1.2. Multi-enriched Pop III descendants

Among the identified three Pop III descendants, we found that two of them are *multi-enriched* by Pop III SNe with different masses and/or different energies:

Boo-119: The measured abundance pattern of the CEMP ($[C/Fe] \approx +2.5$) star Boo-119 (Gilmore et al. 2013) is consistent with 100% *faint* Pop III SNe enrichment (top panel of Fig.6). However, according to our predictions, Boo-119 was enriched by *two* faint Pop III SNe with similar progenitor masses: i) $E_{SN} = 0.3 \times 10^{51}$ erg and $m_\star = 55 M_\odot$ (50%); and ii) $E_{SN} = 0.6 \times 10^{51}$ erg and $m_\star = 58 M_\odot$ (50%). As we can see, our predicted abundance pattern nicely reproduces that observed except for [Ti/Fe], which is commonly underestimated in models compared to observations.

Conversely, the best-fit among all the abundance patterns solely driven by a Pop II SN enrichment, fails to reproduce the observed [C/Fe] value, which is lower by > 1 dex, as well as the [Ca/Fe] and [Cr/Fe] ratios, which exhibit a discrepancy of ~ 0.5 dex.

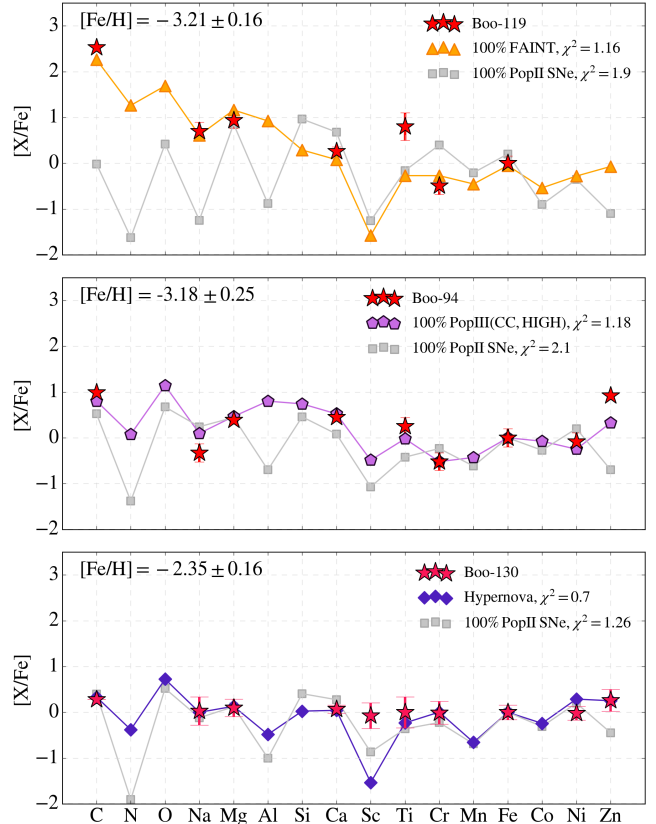


Figure 6. Comparison between the measured abundance patterns of three Boötes I stars classified as *hidden Pop III descendants* (red star symbols) and our best-fits (squares). From top to bottom we show the data of CEMP Boo-119 star (Gilmore et al. 2013), two C-normal stars Boo-94 (Ishigaki et al. 2014) and Boo-94 (Gilmore et al. 2013) and C-low star Boo-130 (Ishigaki et al. 2014). In grey the predicted abundance pattern for an enrichment driven by Pop II stellar population with the chi-square closest to the minimum.

Boo-94: The measured abundance pattern of the Boo-94 star is consistent with 100% enrichment by *three* Pop III SNe with different energies ($\sim 24\%$ by high-energy, $\sim 76\%$ by cc) and masses: two ccSNe with $E_{SN} = 1.2 \times 10^{51}$ erg, and $E_{SN} = 1.5 \times 10^{51}$ erg, and masses respectively equal to $m_\star = 26.5 M_\odot$, and $m_\star = 32 M_\odot$; and one high-energy SNe with $E_{SN} = 3.0 \times 10^{51}$ erg, $m_\star = 27 M_\odot$. Also for this star, the predicted abundance pattern of a 100% Pop II enrichment fails to accurately reproduce the observed abundances in [C/Fe], [Na/Fe], [Ca/Fe], [Ti/Fe] and [Zn/Fe], see Fig.6.

5.2. Ambiguous stars

Within the analyzed Boötes I stars, we have identified a subset that we now classify as “ambiguous”. An example of this is displayed in Fig.7, where we show the comparison between the measured abundance pattern of Boo-1137 (Norris et al. 2010) and the simulated one that produce the best fit. For this star, the minimum $\chi^2 \approx 4.0$ is obtained with an

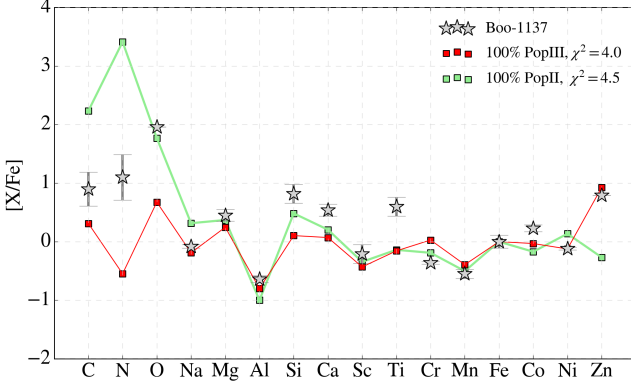


Figure 7. Comparison between the measured abundance pattern of the star Boo-1137 classified as *ambiguous* (grey star symbols, Norris et al. 2010) and our best-fit models (squares) for an enrichment driven by Pop II (green) and by Pop III stellar (red) populations. Note that the Pop II abundance pattern is mainly driven by the contribution of Pop II AGB stars.

enrichment mainly driven by Pop III SNe. However, when plotting the predicted abundance pattern for a 100% Pop II enrichment (with a $> 80\%$ contribution by AGB stars) with a chi-square value very close to the minimum ($\chi^2 \approx 4.5$), we observe that these two abundance patterns appear strikingly similar. Specifically, the two predicted abundance patterns are almost indistinguishable in the Na, Mg, Al, Ca, Sc, Ti, Cr, Mn, Co, and Ni abundances, while they exhibit differences of > 1 dex in C, N, O, and Zn. It is worth noting that this degeneracy could be resolved with the measurement of [N/Fe]. However, nitrogen is both challenging to measure accurately and the surface abundance strongly depends on the stellar evolutionary stage, due to internal stellar mixing processes (e.g. Gratton et al. 2000; Placco et al. 2014).

Why an enrichment driven by 100% Pop III is so similar to 100% Pop II SNe? The reason lies in the number of Pop III SNe progenitors contributing to the ISM pollution. Indeed, upon retrieving the progenitors, we found that this abundance pattern is the result of enrichment from multiple Pop III SNe (> 10), with different masses and energies. Consequently, the distinctive features of individual Pop III SNe are lost resulting in an abundance pattern very similar to that driven by Pop II stars (see Fig. 7).

6. PROBING POP III SUPERNOVA PROPERTIES

In Fig. 8, we show the energies (E_{SN}) and masses (m_{\star}) of the Pop III SNe progenitors for our sample of Pop III descendants (Boo-119, Boo-130, and Boo-94; see Fig. 6). As we can see in the marginal plots, our results probe the existence of Pop III SNe in the mass range $m_{\star} = [20 - 60] M_{\odot}$ and show the coexistence in Boötes I of Pop III descendants with different energies, from faint to hypernovae.

According to our model, the three Pop III SNe descendants have been enriched by a total of two faint, two cc, one high-

energy SN and one hypernovae, i.e. four out of six Pop III progenitors are low-energy SNe. Despite the limited statistics, our findings seem to suggest that Boötes I preferentially retains the chemical elements released by low-energy Pop III SNe. To further explore this aspect, in Fig. 9 we evaluate the percentage of metals, coming from different SNe types, that are locked in stars surviving until $z = 0$. Given that Boötes I is currently a gas-free galaxy, this percentage also reflects the metals retained by its gravitational potential well throughout its evolution.

The first thing to note is that the fraction of metals retained by stars is always very small, $\lesssim 2.5\%$, the maximum corresponding to the case of Pop II SNe. The percentage is even lower for Pop III SNe, less than $\lesssim 1.1\%$ of metals retained. Moreover, for Pop III SNe, there is clear trend with explosion energy: the fraction of metals retained is greater $\gtrsim 1\%$ for low-energy SNe (faint, cc) but decreases as the energy increases. Finally, in Fig. 9 we also show the fraction of metals retained by Boötes I when PISN explode. As observed, the fraction is $< 0.1\%$. This is attributed to two distinct effects: firstly, the random sampling of the IMF plays a fundamental role. Indeed, when the first stars form, the star-formation rate is low (less than $10^{-2} M_{\odot} \text{yr}^{-1}$, see Rossi et al. 2021), making the formation of stars in the PISN mass range, i.e., $[140 - 260] M_{\odot}$, less probable. Secondly, when PISNe explode, they are so energetic that they blow out all the gas within the galaxy. Only in the case of low-mass PISNe ($m_{\star} \sim 140 M_{\odot}$) evolving, a fraction of the metals injected into the ISM can be retained by Boötes I, however the probability to form them is very low. We can conclude that the probability to find the imprint of PISN in UFDs is extremely low due to their shallow potential wells.

7. DISCUSSION

The approach of comparing observed and simulated abundance patterns to determine the properties of progenitors of metal-poor stars is widely used. However, this approach typically involves fitting the observed abundance patterns with the yields from a single Pop III SN (e.g. Heger & Woosley 2010; Ishigaki et al. 2018) or a few (e.g. Hartwig et al. 2018; Welsh et al. 2023) Pop III progenitors. Finding stars enriched by a single Pop III SNe is exciting, but we have demonstrated that such stars are expected to be extremely rare even in ancient and metal-poor UFDs. The majority of Pop III descendants are expected to be enriched by multiple progenitors, with different masses and energy, each contributing to the observed abundance patterns with different percentage (see Sec. 5.1). Therefore, it is crucial to interpret these data using *self-consistent* chemical evolution models that account for the different sources of enrichment. We show that identifying Pop III descendants is possible, though challenging, and that some may be hidden in existing literature data.

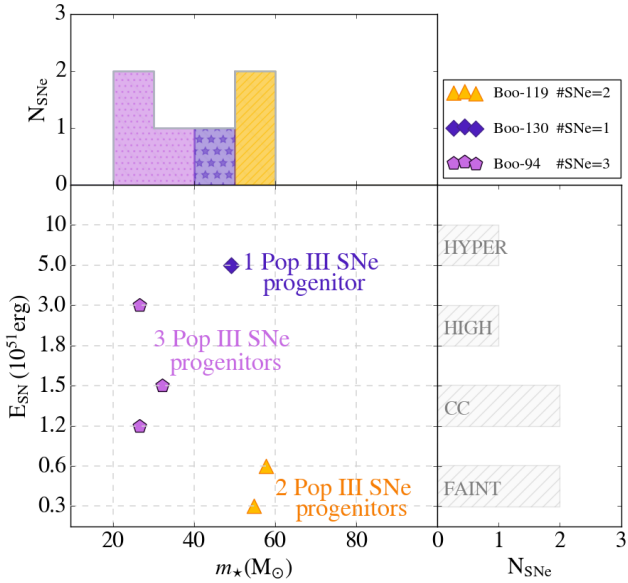


Figure 8. The energy-mass ($E_{\text{SN}}-m_{\star}$) distribution of Pop III SNe progenitors of Boötes I stars. The two multi-enriched first stars descendants Boo-119 (orange) and Boo-94 (purple); and a mono-enriched Pop III descendant Boo-130 (blue). Marginal plots show the number of SNe (N_{SNe}) as a function of m_{\star} (top) and E_{SN} (right).

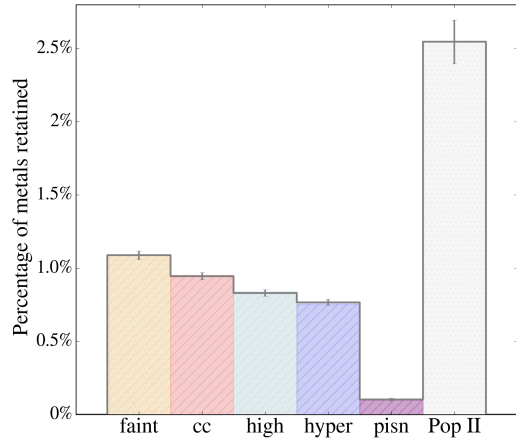


Figure 9. The fraction of metals retained in the potential well of Boötes I galaxy after the explosion of different SNe type: faint (orange), cc (red), high-energy (light blue), hypernovae (blue), PISN (purple), Pop II SNe (grey).

Among the 42 Boötes I stars with measured chemical abundance ratios, three are consistent with being direct Pop III descendants. Notably, two of these three stars are multi-enriched by Pop III SNe with different energies and masses (see Sec.5.1). On the other hand, our results show that if the gas has been enriched by more than 10 Pop III SNe, the resulting abundance pattern does not display the distinctive chemical features of Pop III descendants. Instead, it becomes indistinguishable from that produced by Pop II stars (see Sec.5.2). Boo-1137 is a perfect example of this case

(see Fig.7), where we cannot discriminate between enrichment driven by a Pop III or Pop II stellar population. This star was also analyzed by Welsh et al. (2023), who found that Boo-1137 had been enriched by a single Pop III progenitor with $m_{\star} = (18 - 27) M_{\odot}$. It is important to note that to achieve this result, the authors used only five chemical elements (C, O, Al, Si, Fe), while for Boo-1137, there are 11 other measured chemical elements in the literature that we used to determine the best-fit model. We can speculate that the different interpretation of the origin of this Boo-1137 is due to the number of chemical abundance ratios used in the analysis. This discrepancy emphasizes the importance of employing a wide range of chemical elements (> 5) to accurately interpret data and to give constraints on the initial metallicity, mass and explosion energy of the progenitor stars imprinting the birth environment.

For direct Pop III descendants we infer the mass of their progenitors that is in mass range $m_{\star} = [20 - 60] M_{\odot}$. These results are partially in agreement with the results of Ishigaki et al. (2018). The authors found that the abundance patterns of extremely metal-poor stars ($[\text{Fe}/\text{H}] < -3$) are predominantly best-fitted by SNe yields with $m_{\star} < 40 M_{\odot}$ and that more than half of the stars are best-fitted by the $m_{\star} = 25 M_{\odot}$ hypernova ($E = 10 \times 10^{51} \text{ erg}$) models. Finally they conclude that the masses of Pop III stars responsible for the first metal enrichment are predominantly $m_{\star} < 40 M_{\odot}$. On the other hand, our results suggest that the masses of Pop III stars responsible of the enrichment are higher, up to $\approx 60 M_{\odot}$. Note that Ishigaki et al. (2018) use different sets of stellar yields (see their Sec.2) and they have, for $m_{\star} > 25 M_{\odot}$, only two stellar model yields for stars with $m_{\star} = 40 M_{\odot}$ and $m_{\star} = 100 M_{\odot}$ (see Table 1 in Ishigaki et al. 2018). While we used the stellar yields of Heger & Woosley (2010) that have more stellar models within this range.

Finally, our results show that UFDs are strongly affected by SNe feedback processes (Fig. 9). In particular, we show that the chemical products of energetic PISN are completely lost by Boötes I, which is hosted by a $\approx 10^7 M_{\odot}$ mini-halo. This is in perfect agreement with simulations of Pop III SNe in high-z low-mass minihalos (Bromm et al. 2002; Ritter et al. 2012; Smith et al. 2015). To quantitatively compare our predictions with other studies for nearby dwarf galaxies we evaluate the mass-loading factor⁵, $\eta = 85 \pm 12$ that is in good agreement with the results of Sandford et al. (2024) and with hydrodynamic simulations (e.g. Emerick 2019; Pandya et al. 2021).

⁵ $\eta = \dot{M}_{ej}/\dot{M}_{\star}$, defined as the ratio between the rate of ejected mass and star formation rate.

8. CONCLUSIONS

To investigate the chemical signatures left by Pop III SNe, we implement a theoretical chemical evolution model of Boötes I (Rossi et al. 2021, 2023), the best studied UFD galaxy. Our model accounts for the incomplete sampling of the IMF in this poorly star-forming system. The chemical enrichment from carbon to zinc is followed by including SNe and AGB stars from both Pop III stars and the subsequent Pop II stellar populations. Our key results are:

- To accurately reproduce the measured abundance ratios in Boötes I stars (in particular [C/Fe] and [Zn/Fe]), it is necessary to include contribution of Pop III SNe with *both low and high energies* (Fig.3). Consequently, in our “fiducial model” we adopt a theoretical EDF which is distributed among different equiprobable energies (faint, cc, high-energy and hypernovae), see Fig.1.
- In [X/Fe] vs [Fe/H] diagrams, true Pop III descendants can be identified within low-density regions as *outliers* (see Fig.4). In particular, stars at $[Fe/H] < -4$ with $[C/Fe] \gtrsim +1$ or $[C/Fe] \lesssim 0$, $[Mg/Fe] \gtrsim +0.5$, $[Na/Fe] \gtrsim +0.5$, $[Si/Fe] \gtrsim +1$, $[Ca/Fe] \gtrsim +0.5$, $[Ni/Fe] \gtrsim +0.5$ or $[Zn/Fe] \lesssim -1$, have a higher probability to be Pop III descendants.
- The [C/Fe] ratio is a *key abundance ratio* to unveil the descendants of Pop III SNe. We show that at $[Fe/H] < -3$ we can find the imprint of Pop III SNe with explosion energies $E_{SN} = [0.3 - 3] \times 10^{51}$ erg, i.e. faint, cc, high-energy Pop III SNe among CEMP stars (Fig.5). While the chemical signature of hypernovae arises at $[Fe/H] > -3.5$ among C-normal stars with $[C/Fe] < +0.7$.
- Among literature data of Boötes I stars with > 5 abundance ratios measured, we uncover *one mono-enriched and two multi-enriched Pop III descendants* (Fig.6). Specifically, our findings show that the CEMP star Boo-119 exhibits an abundance pattern consistent with enrichment by two faint Pop III SNe; Boo-94 formed in an environment polluted by three Pop III SNe (two ccSN and one high-energy SN); and, notably, we identify a mono-enriched Pop III hypernova

descendant, Boo-130;

- Retrieving properties of the progenitors of Pop III descendants we found that they have masses in the range $[20 - 60] M_\odot$ and *different energies* spanning from low to high energy (Fig.8).
- Examining the chemical evolution of Boötes I, we found that in UFDs the fraction of metals retained by their gravitational potential is very low ($\lesssim 2.5\%$) independent of the SNe type. For low-energy Pop III SNe the fraction is $\approx 1\%$, while it is even lower for more energetic Pop III SNe (Fig.9).
- Finding the chemical signatures of energetic PISNe is unlikely in systems like UFDs, as the fraction of metals retained by their potential wells is $\lesssim 0.2\%$ (Fig.9).

To delve deeper into unraveling the mysteries of Pop III SNe, such as their energy and mass properties, it is crucial to identify their descendants and measure their chemical properties. Our analysis demonstrates that for understanding the chemical evolution of Boötes I it is vital to consider different Pop III SNe types, whose direct descendants can be identified as *outliers* in different chemical abundance spaces. Overall, our study offers a robust framework for interpreting observational data in Boötes I, allowing for the identification of Pop III descendants based on their chemical signatures. In conclusion, our model stands ready to analyze and interpret upcoming data like 4MOST/4DWARFS (Skúladóttir et al. 2023), providing a comprehensive understanding of the properties of the first supernovae.

9. ACKNOWLEDGMENTS

¹ This project has received funding from the European Research Council (ERC) under the European Union’s Horizon 2020 research and innovation programme (grant agreement No 804240). S.S. and I.V. acknowledge support from the PRIN-MIUR2017, prot. n. 2017T4ARJ5. Á.S. acknowledges ERC support (grant agreement No. 101117455).

APPENDIX

A. THE PROBABILITY TO FIND POP III DESCENDANTS

The [C/Fe] ratio is commonly used as a diagnostic tool for identifying metal-poor stars enriched by Pop III sources. Additionally, the A(C) value is employed to discern the origins of distinct CEMP stellar populations: in Rossi et al. (2023) we show that among CEMP-no stars, true Pop III stars *descendants* appear for $A(C) \lesssim 6$ and $[Fe/H] \lesssim -3.5$.

To unveil if there exists a region in which Pop III descendants can be found, we derived the probability that a given stellar population has been imprinted by Pop III or Pop II SNe for different $[Fe/H]$ and $[C/Fe]$ (or $A(C)$) values. By inspecting the $A(C)$ - $[Fe/H]$ diagram in Fig.10 it is evident that two separate branches exist, both showing roughly constant $A(C)$ values in the $[Fe/H]$ range. The first branch, at $A(C) \approx 7$ is dominated by stars predominantly enriched by Pop II stars. In the second branch, $A(C) \lesssim 6$, the enrichment is driven by Pop III SNe. The two different branches are also evident in $[C/Fe]$ - $[Fe/H]$ space where we can note that Pop III and Pop II enriched stars are located in two parallel branches that exhibit a strong correlation with $[Fe/H]$. As already discussed in Rossi et al. 2023, Pop II enriched stars can be divided into two different groups with different chemical enrichment sources: stellar populations with $[C/Fe] > +0.7$ and $[Fe/H] \lesssim -4$, located in the branch at $A(C) \gtrsim 7$, are the so called *moderate CEMP* stars, which formed from an ISM mainly enriched by Pop II AGB stars. C-normal stars with $[C/Fe] \lesssim +0.7$ and $-4 \lesssim [Fe/H] \lesssim -1$ form in birth clouds predominantly enriched by Pop II SNe. Indeed, Pop II SNe stellar yields adopted (Limongi & Chieffi 2018), do not allow to form stellar populations enhanced in carbon, i.e. with $[C/Fe] > +0.7$. Finally, carbon-enhanced stars with $-3.5 \lesssim [Fe/H] \lesssim -1$ formed out of gas enriched by both AGB and SNe Pop II stars. Pop III enriched stars are located in the low-branch at $A(C) \lesssim 6$ of the $A(C)$ - $[Fe/H]$ or equivalently in the bottom branch of the $[C/Fe]$ - $[Fe/H]$ diagram. The majority of Pop III stars descendants with $[Fe/H] < -4$ are CEMP-no stars and the probability to find them increases as $[Fe/H]$ decreases and it is maximum for $A(C) \lesssim 6$ and $[Fe/H] \lesssim -3.5$. Furthermore, it is predicted that Pop III descendants can be found among C-normal stars. In particular at $[C/Fe] < 0$ and $-4 \lesssim [Fe/H] \lesssim -1$ the probability to find the chemical signatures of pristine SNe exceeds $\gtrsim 50\%$. In conclusion, by exploiting both $[C/Fe]$ and $A(C)$ as diagnostics we can successfully predict promising descendants among both CEMP and C-normal stars: carbon-enhanced Pop III stars descendants are predicted to have $A(C) \lesssim 6$ and $[Fe/H] \lesssim -3.5$ while C-normal stars imprinted by Pop III SNe have $[C/Fe] < 0$ and $[Fe/H] \gtrsim -3.5$. In other words we predict that stars with these properties have the highest probability of being Pop III descendants.

B. POP II DESCENDANTS

- **Boo-009, Boo-33, Boo-127** - We analysed the abundance pattern of Boo-009 (Ishigaki et al. 2014), Boo-33 (Gilmore et al. 2013) and Boo-127 (Ishigaki et al. 2014) (Fig.11). The first thing to note is that the abundance patterns measured for these stars are very similar. Furthermore, they are in agreement with an enrichment predominantly driven by Pop II SNe, accounting for 51% in the best model for Boo-009, 82% for Boo-33, and 85% for Boo-127. While Boo-009 is a pure Pop II enriched star that has been also enriched (at 49%) by Pop II AGB, it is worth noting that both of Boo-33 and Boo-127 experienced some level of enrichment from Pop III SNe hypernovae and core-collapse, which, however, did not leave particularly distinct signatures in their abundance patterns.

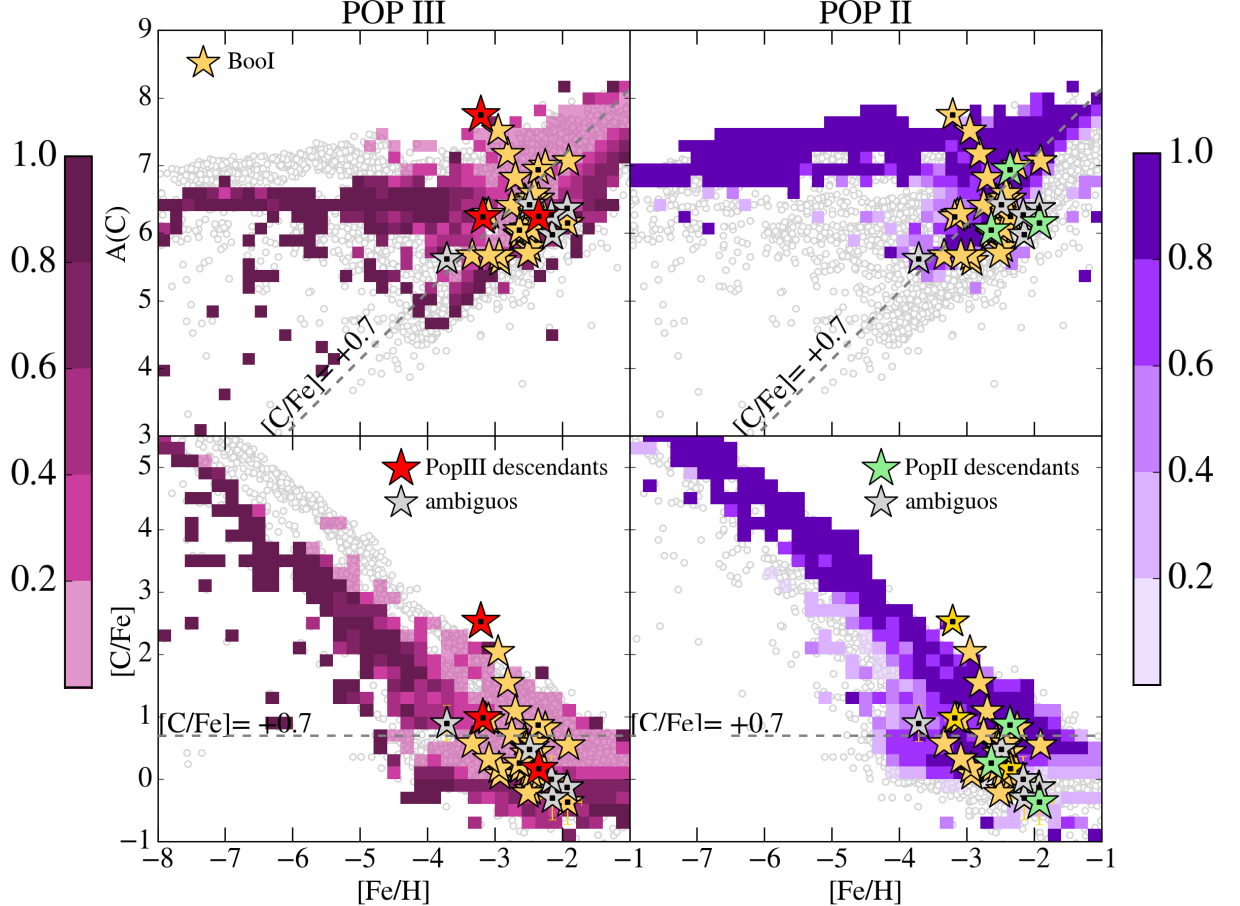


Figure 10. The $A(C)$ (top panel) and $[C/Fe]$ (bottom panel) versus $[Fe/H]$ diagram for Boötes I stellar populations. The colored squares identify the probability to find, at fixed $[Fe/H]$ and $A(C)$ (of $[C/Fe]$), stars predominantly enriched by Pop III or by Pop II stars (columns). Star points represent the Boötes I data where the ones with a square in their center identify the stars for which the abundance ratio of different chemical elements is available in the literature. The different color of Boötes I stars represent Pop III descendants (red, Sec.5.1), Pop II descendants (green, Sec.B) and “ambiguous” stars (grey) for which it is not possible discriminate their origin, respectively (see Sec.5.2).

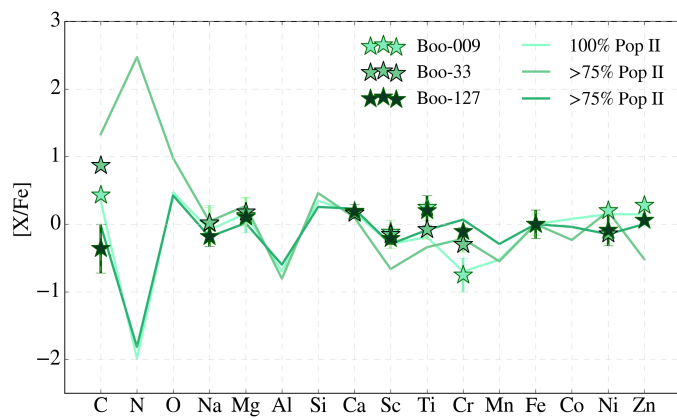


Figure 11. Comparison between the observed (star symbols) and the best-fit (lines) abundance pattern of Boo-009, Boo-33, and Boo-127 (Gilmore et al. 2013; Ishigaki et al. 2014).

REFERENCES

- Abel, T., Bryan, G. L., & Norman, M. L. 2002, *Science*, 295, 93, doi: [10.1126/science.295.5552.93](https://doi.org/10.1126/science.295.5552.93)
- Aguado, D. S., Caffau, E., Molnar, P., et al. 2023, *A&A*, 669, L4, doi: [10.1051/0004-6361/202245392](https://doi.org/10.1051/0004-6361/202245392)
- Asplund, M., Grevesse, N., Sauval, A. J., & Scott, P. 2009, *ARA&A*, 47, 481, doi: [10.1146/annurev.astro.46.060407.145221](https://doi.org/10.1146/annurev.astro.46.060407.145221) [10.48550/arXiv.0909.0948](https://arxiv.org/abs/0909.0948)
- Barkana, R., & Loeb, A. 2001, *Physics reports*, 349, 125
- Beers, T. C., & Christlieb, N. 2005, *Annu. Rev. Astron. Astrophys.*, 43, 531
- Bonifacio, P., Caffau, E., Spite, M., et al. 2015, *Astronomy & Astrophysics*, 579, A28
- Bromm, V. 2013, *Reports on Progress in Physics*, 76, 112901
- Bromm, V., Coppi, P. S., & Larson, R. B. 2002, *ApJ*, 564, 23, doi: [10.1086/323947](https://doi.org/10.1086/323947)
- Bromm, V., Ferrara, A., Coppi, P., & Larson, R. 2001, *Monthly Notices of the Royal Astronomical Society*, 328, 969
- Brown, T. M., Tumlinson, J., Geha, M., et al. 2014, *The Astrophysical Journal*, 796, 91
- de Bennassuti, M., Salvadori, S., Schneider, R., Valiante, R., & Omukai, K. 2017, *Monthly Notices of the Royal Astronomical Society*, 926
- Emerick, A. J. 2019, PhD thesis, Columbia University, New York
- Ezzeddine, R., Frebel, A., Roederer, I. U., et al. 2019, *ApJ*, 876, 97, doi: [10.3847/1538-4357/ab14e7](https://doi.org/10.3847/1538-4357/ab14e7)
- Fu, S. W., Weisz, D. R., Starkenburg, E., et al. 2023, *ApJ*, 958, 167, doi: [10.3847/1538-4357/ad0030](https://doi.org/10.3847/1538-4357/ad0030)
- Gallart, C., Monelli, M., Ruiz-Lara, T., et al. 2021, arXiv e-prints, arXiv:2101.04464. <https://arxiv.org/abs/2101.04464>
- Gilmore, G., Norris, J. E., Monaco, L., et al. 2013, *The Astrophysical Journal*, 763, 61
- Gratton, R. G., Sneden, C., Carretta, E., & Bragaglia, A. 2000, *A&A*, 354, 169
- Greif, T., Springel, V., White, S., et al. 2011, arXiv preprint arXiv:1101.5491
- Hartwig, T., Bromm, V., Klessen, R. S., & Glover, S. C. 2015, *Monthly Notices of the Royal Astronomical Society*, 447, 3892
- Hartwig, T., & Yoshida, N. 2019, *ApJL*, 870, L3, doi: [10.3847/2041-8213/aaf866](https://doi.org/10.3847/2041-8213/aaf866)
- Hartwig, T., Yoshida, N., Magg, M., et al. 2018, *MNRAS*, 478, 1795, doi: [10.1093/mnras/sty1176](https://doi.org/10.1093/mnras/sty1176)
- Heger, A., & Woosley, S. E. 2002, *The Astrophysical Journal*, 567, 532
- Heger, A., & Woosley, S. E. 2010, *ApJ*, 724, 341, doi: [10.1088/0004-637X/724/1/341](https://doi.org/10.1088/0004-637X/724/1/341)
- Hirano, S., & Bromm, V. 2017, *MNRAS*, 470, 898, doi: [10.1093/mnras/stx1220](https://doi.org/10.1093/mnras/stx1220)
- Hirano, S., Hosokawa, T., Yoshida, N., et al. 2014, *The Astrophysical Journal*, 781, 60
- Ishigaki, M. N., Aoki, W., Arimoto, N., & Okamoto, S. 2014, *A&A*, 562, A146, doi: [10.1051/0004-6361/201322796](https://doi.org/10.1051/0004-6361/201322796)
- Ishigaki, M. N., Tominaga, N., Kobayashi, C., & Nomoto, K. 2018, *The Astrophysical Journal*, 857, 46
- Iwamoto, N., Umeda, H., Tominaga, N., Nomoto, K., & Maeda, K. 2005, *Science*, 309, 451, doi: [10.1126/science.1112997](https://doi.org/10.1126/science.1112997)
- Karlsson, T., Bromm, V., & Bland-Hawthorn, J. 2013, *Reviews of Modern Physics*, 85, 809
- Kirby, E. N., Cohen, J. G., Guhathakurta, P., et al. 2013, *The Astrophysical Journal*, 779, 102
- Klessen, R. S., & Glover, S. C. O. 2023, *ARA&A*, 61, 65, doi: [10.1146/annurev-astro-071221-053453](https://doi.org/10.1146/annurev-astro-071221-053453)
- Kobayashi, C., Umeda, H., Nomoto, K., Tominaga, N., & Ohkubo, T. 2006, *ApJ*, 653, 1145, doi: [10.1086/508914](https://doi.org/10.1086/508914)
- Koutsouridou, I., Salvadori, S., & Skúladóttir, Á. 2024, *ApJL*, 962, L26, doi: [10.3847/2041-8213/ad2466](https://doi.org/10.3847/2041-8213/ad2466)
- Koutsouridou, I., Salvadori, S., Skúladóttir, Á., et al. 2023, *MNRAS*, 525, 190, doi: [10.1093/mnras/stad2304](https://doi.org/10.1093/mnras/stad2304)
- Lai, D. K., Lee, Y. S., Bolte, M., et al. 2011, *The Astrophysical Journal*, 738, 51
- Larson, P. L. 1998, *Gaia*, 15, 389
- Limongi, M., & Chieffi, A. 2018, *VizieR Online Data Catalog*, J/ApJS/237/13
- Magg, M., Hartwig, T., Agarwal, B., et al. 2017, *Monthly Notices of the Royal Astronomical Society*, 473, 5308
- Magg, M., Klessen, R. S., Glover, S. C. O., & Li, H. 2019, *MNRAS*, 487, 486, doi: [10.1093/mnras/stz1210](https://doi.org/10.1093/mnras/stz1210)
- Meynet, G., & Maeder, A. 2002, *A&A*, 390, 561, doi: [10.1051/0004-6361:20020755](https://doi.org/10.1051/0004-6361:20020755)
- Norris, J. E., Yong, D., Gilmore, G., & Wyse, R. F. 2010, *The Astrophysical Journal*, 711, 350
- Omukai, K., & Palla, F. 2001, *ApJL*, 561, L55, doi: [10.1086/324410](https://doi.org/10.1086/324410)
- Omukai, K., Tsuribe, T., Schneider, R., & Ferrara, A. 2005, *The Astrophysical Journal*, 626, 627, doi: [10.1086/429955](https://doi.org/10.1086/429955)
- Pagnini, G., Salvadori, S., Rossi, M., et al. 2023, *MNRAS*, doi: [10.1093/mnras/stad912](https://doi.org/10.1093/mnras/stad912)
- Pandya, V., Fielding, D. B., Anglés-Alcázar, D., et al. 2021, *Monthly Notices of the Royal Astronomical Society*, 508, 2979
- Placco, V. M., Frebel, A., Beers, T. C., & Stancliffe, R. J. 2014, *ApJ*, 797, 21, doi: [10.1088/0004-637X/797/1/21](https://doi.org/10.1088/0004-637X/797/1/21)
- Placco, V. M., Roederer, I. U., Lee, Y. S., et al. 2021, *ApJL*, 912, L32, doi: [10.3847/2041-8213/abf93d](https://doi.org/10.3847/2041-8213/abf93d)
- Planck Collaboration, Aghanim, N., Akrami, Y., et al. 2018, arXiv e-prints, arXiv:1807.06209. <https://arxiv.org/abs/1807.06209>
- Prole, L. R., Clark, P. C., Klessen, R. S., Glover, S. C. O., & Pakmor, R. 2022, *MNRAS*, 516, 2223, doi: [10.1093/mnras/stac2327](https://doi.org/10.1093/mnras/stac2327)

- Riaz, R., Schleicher, D. R. G., Bovino, S., Vanaverbeke, S., & Klessen, R. S. 2023, MNRAS, 518, 4895, doi: [10.1093/mnras/stac3310](https://doi.org/10.1093/mnras/stac3310)
- Ritter, J. S., Safranek-Shrader, C., Gnat, O., Milosavljević, M., & Bromm, V. 2012, ApJ, 761, 56, doi: [10.1088/0004-637X/761/1/56](https://doi.org/10.1088/0004-637X/761/1/56)
- Rossi, M., Salvadori, S., & Skúladóttir, Á. 2021, MNRAS, 503, 6026, doi: [10.1093/mnras/stab821](https://doi.org/10.1093/mnras/stab821)
- Rossi, M., Salvadori, S., Skúladóttir, Á., & Vanni, I. 2023, MNRAS, 522, L1, doi: [10.1093/mnrasl/slad029](https://doi.org/10.1093/mnrasl/slad029)
- Salvadori, S., Bonifacio, P., Caffau, E., et al. 2019, Monthly Notices of the Royal Astronomical Society, 487, 4261
- Salvadori, S., & Ferrara, A. 2009, Monthly Notices of the Royal Astronomical Society: Letters, 395, L6
- Salvadori, S., Ferrara, A., & Schneider, R. 2008, Monthly Notices of the Royal Astronomical Society, 386, 348
- Salvadori, S., Schneider, R., & Ferrara, A. 2007, Monthly Notices of the Royal Astronomical Society, 381, 647
- Salvadori, S., Skuladottir, A., & Tolstoy, E. 2015, Monthly Notices of the Royal Astronomical Society, 454, 1320
- Sandford, N. R., Weinberg, D. H., Weisz, D. R., & Fu, S. W. 2024, MNRAS, 530, 2315, doi: [10.1093/mnras/stae1010](https://doi.org/10.1093/mnras/stae1010)
- Sarmento, R., Scannapieco, E., & Côté, B. 2019, ApJ, 871, 206, doi: [10.3847/1538-4357/aafa1a](https://doi.org/10.3847/1538-4357/aafa1a)
- Schneider, R., Ferrara, A., Salvaterra, R., Omukai, K., & Bromm, V. 2003, Nature, 422, 869, doi: [10.1038/nature01579](https://doi.org/10.1038/nature01579)
- Sharda, P., Federrath, C., Krumholz, M. R., & Schleicher, D. R. G. 2021, MNRAS, 503, 2014, doi: [10.1093/mnras/stab531](https://doi.org/10.1093/mnras/stab531)
- Simon, J. D. 2019, Monthly Notices of the Royal Astronomical Society
- Skúladóttir, Á., Koutsouridou, I., Vanni, I., et al. 2024, arXiv e-prints, arXiv:2404.19086, doi: [10.48550/arXiv.2404.19086](https://doi.org/10.48550/arXiv.2404.19086)
- Skúladóttir, Á., Salvadori, S., Amarsi, A. M., et al. 2021, ApJL, 915, L30, doi: [10.3847/2041-8213/ac0dc2](https://doi.org/10.3847/2041-8213/ac0dc2)
- Skúladóttir, Á., Puls, A. A., Amarsi, A. M., et al. 2023, The Messenger, 190, 19, doi: [10.18727/0722-6691/5304](https://doi.org/10.18727/0722-6691/5304)
- Smith, B. D., Wise, J. H., O'Shea, B. W., Norman, M. L., & Khochfar, S. 2015, MNRAS, 452, 2822, doi: [10.1093/mnras/stv1509](https://doi.org/10.1093/mnras/stv1509)
- Spite, M., Spite, F., François, P., et al. 2018, A&A, 617, A56, doi: [10.1051/0004-6361/201833548](https://doi.org/10.1051/0004-6361/201833548)
- Suda, T., Katsuta, Y., Yamada, S., et al. 2008, PASJ, 60, 1159, <https://arxiv.org/abs/0806.3697>
- Susa, H., Hasegawa, K., & Tominaga, N. 2014, The Astrophysical Journal, 792, 32
- Takahashi, K., Yoshida, T., & Umeda, H. 2018, ApJ, 857, 111, doi: [10.3847/1538-4357/aab95f](https://doi.org/10.3847/1538-4357/aab95f)
- Tan, J. C., & McKee, C. F. 2004, ApJ, 603, 383, doi: [10.1086/381490](https://doi.org/10.1086/381490)
- Thibodeaux, P. N., Ji, A. P., Cerny, W., Kirby, E. N., & Simon, J. D. 2024, arXiv e-prints, arXiv:2404.17078, doi: [10.48550/arXiv.2404.17078](https://doi.org/10.48550/arXiv.2404.17078)
- van den Hoek, L. B., & Groenewegen, M. A. T. 1997, A&AS, 123, 305, doi: [10.1051/aas:1997162](https://doi.org/10.1051/aas:1997162)
- Vanni, I., Salvadori, S., Skúladóttir, Á., Rossi, M., & Koutsouridou, I. 2023, MNRAS, 526, 2620, doi: [10.1093/mnras/stad2910](https://doi.org/10.1093/mnras/stad2910)
- Welsh, L., Cooke, R., Fumagalli, M., & Pettini, M. 2023, MNRAS, 525, 527, doi: [10.1093/mnras/stad2181](https://doi.org/10.1093/mnras/stad2181)
- Xing, Q.-F., Zhao, G., Liu, Z.-W., et al. 2023, Nature, 618, 712, doi: [10.1038/s41586-023-06028-1](https://doi.org/10.1038/s41586-023-06028-1)
- Yong, D., Norris, J. E., Bessell, M. S., et al. 2013, ApJ, 762, 26, doi: [10.1088/0004-637X/762/1/26](https://doi.org/10.1088/0004-637X/762/1/26)
- Yoon, J., Beers, T. C., Tian, D., & Whitten, D. D. 2019, ApJ, 878, 97, doi: [10.3847/1538-4357/ab1ead](https://doi.org/10.3847/1538-4357/ab1ead)